Center for Turbulence Research
Proceedings of the Summer Program 2008

LES of the trailing-edge flow and noise of a NACA6512-63 airfoil at zero angle of attack

By J. Winkler† AND S. Moreau‡

Large-eddy simulations (LES) of flow over a low-speed highly cambered airfoil at small negative incidence is performed using two different flow solvers, CFX and Fluent, on a similar multi-block structured mesh. They mimic recent aeroacoustic experiments performed in the small anechoic wind tunnel at the University of Siegen. Focus has been put on the experiments where the airfoil was tripped to remove the extraneous Tollmien-Schlichting noise source. Two different tripping models have been simulated, where the actual serrated device is found to trigger the transition correctly as in the experiment. The LES and Reynolds-averaged Navier-Stokes (RANS) $k-\omega$ SST simulations are also compared with detailed velocity measurements made by a 3-D hot-wire in the wake. The LES predicts the wake thickness and deficit much better than the RANS and is the only one to yield the flow separation at the trailing edge. The acoustic predictions from two formulations of Lighthill's acoustic analogy compare favorably with the anechoic wind tunnel measurements at low and mid-frequencies. The formulation by Ffowcs Williams & Hall (1970) shows better agreement with the tripped boundary layer experiments, whereas Curle's (1955) analogy predicts the untripped airfoil sound radiation better.

1. Introduction

The trailing-edge noise of an airfoil is again considered as described by Christophe & Moreau (2008). Yet a NACA6512-63 airfoil, which is a highly cambered airfoil more typical of highly loaded, high-speed turbo-engine compressors is presently used. The flow condition is also very different from the named case as this airfoil is set to a 0° angle of attack with respect to the chord line (α_w in Moreau *et al.* (2003)). This corresponds to an operating condition at high mass flow rate, beyond the design condition previously studied on the Valeo Controlled-Diffusion airfoil (Moreau *et al.* 2004, Moreau *et al.* 2005, Moreau *et al.* 2006). This also triggers an effective negative incidence with respect to the airfoil mean line at the leading edge. For this particular flow condition, large laminar flow regions exist around the airfoil and Tollmien-Schlichting waves develop on both pressure and suction sides of the airfoil, which yields extraneous far-field noise characterized by typical broadband humps on which regular tones are superimposed (Arbey & Bataille, 1983). To remove this additional noise source, one can resort to boundary-layer tripping. As shown by Hama (1957), the most efficient trip is a thin forward-facing serration applied close to the leading edge on both airfoil sides. This is what has been tested both experimentally and numerically in the present study.

The experimental investigation performed at the University of Siegen is first summarized in the next section. The collected data so far involve lift and wake velocity measurements, as well as far-field acoustic data. The complete experimental setup is then simulated in Sec. 3. Two LES computations, using the commercial codes Fluent

† University of Siegen, Siegen, Germany
‡ Valeo Thermal Systems, 78321 La Verrière, France

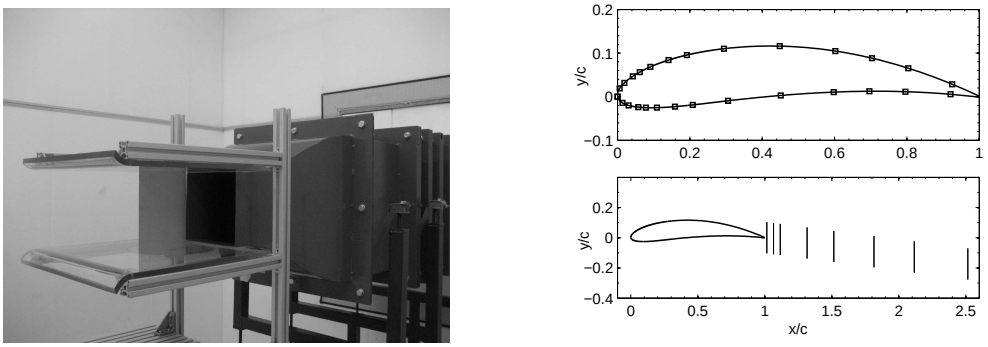

FIGURE 1. Left: Exerimental setup in front of the wind tunnel at the University of Siegen. Right: Locations for lift measurements on the NACA6512-63 airfoil (top) and wake velocity measurements (bottom).

and CFX are performed with two different tripping models. A simplified stair step is implemeted in CFX. However the results presented here are focused on the Fluent case, which incorporates the actual experimental boundary-layer serrations in the numerical grid. The results of the Fluent-LES are then compared with the experimental data in Sec. 4, including a first comparison with the simplified boundary layer stair-step case. Finally, acoustic predictions based on Curle's and Ffowcs Williams-Hall's models are made in the last section.

2. Experimental database

Experiments have been conducted in the small aeroacoustic wind tunnel facility at the University of Siegen. The facility is equipped with a muffler and several screen and honeycomb combinations to obtain a flat velocity profile at the nozzle exit with turbulence intensities below 0.4%. It terminates in an anechoic chamber, to allow for acoustic measurements. A detailed description of the facility can be found in Winkler & Carolus (2008). The NACA6512-63 airfoil mock-up has a 13.5 cm constant chord length (c) and an 18 cm span (L). It is placed 0.56 c downstream from the nozzle exit plane. It is held between two horizontal side plates fixed to the nozzle of the open-jet wind tunnel as shown in Fig. 1 (left). These plates are 18 cm ($\approx$1.33 c) apart and the width of the rectangular jet is 18 cm. The chord-based Reynolds number of the flow is $Re_c = 1.9\times10^5$. The Mach number is 0.062. The angle of attack with respect to the chord, α_w, is 0°. This small incidence has been selected to limit the jet deflection and the interaction of the shear layers coming from the nozzle lips with the airfoil.

The NACA6512-63 airfoil mock-up is equipped at midspan with 27 flush-mounted remote microphone probes (RMP), which measure both the mean and fluctuating pressure within a frequency range of 20 Hz–25 kHz. Figure 1 (right) shows the layout of the streamwise wall pressure measurement locations at the midspan plane of the airfoil, and the eight planes in the airfoil wake where velocity measurements have been made by a 3-D hot-wire. For each plane, data have been acquired at a minimum of 50 points.

Acoustic measurements have been made by three microphones at a distance of 1.2 m from the trailing edge under different observer angles. A cross-correlation technique, as described by Blake & Lynch (2002) and Winkler & Carolus (2008), between the microphone signals has been implemented to extract the trailing-edge noise from the facility background noise. It has been found that at the present Reynolds number, Tollmien-

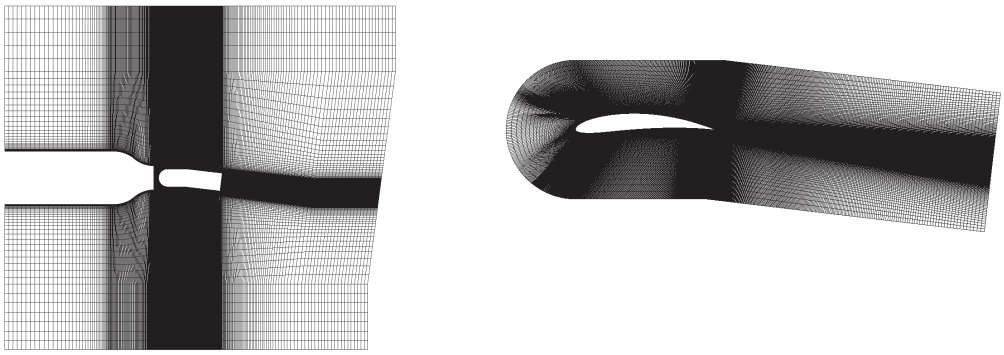

FIGURE 2. Left: Grid topology of the wind tunnel setup in Siegen for initial RANS computations. Right: LES truncated domain, extracted from the full wind tunnel setup.

Schlichting instability waves occur in the laminar boundary layer which lead to additional sound radiation, including tonal noise components. In order to suppress these instabilities and the associated sound radiation, the boundary layer of the airfoil had been tripped on both sides at 10% chord by a serrated aluminum tape of thickness 80 μm as suggested by Hama (1957). This trip covers the whole span and has been found to pose the least, but yet sufficient disturbance to the boundary layer to obtain transition for the given Reynolds number.

3. Large-eddy simulations for the NACA6512-63 airfoil

3.1. *Flow solvers*

The LES is based on the spatially filtered, incompressible Navier-Stokes equations with the dynamic subgrid-scale model (Germano *et al.* 1991; Lilly 1992). They are solved with two commercial codes, CFX and Fluent from ANSYS. In the former, the governing equations are solved with a control-volume-based finite element method. Central differencing is used for the spatial discretization. Time integration is made with an implicit scheme. In the latter, the governing equations are solved with a classical finite volume method. A central-difference scheme is similarly used for the spatial discretization and the non-iterative time-advancement (NITA) scheme is used for the time advancement. Therefore in both cases, solutions are second-order accurate in space and time. The present LES use CFX-11 and Fluent 6.3 versions.

Preliminary RANS computations are required for generating the LES boundary conditions, as described in the next section. They have been performed using the Shear-Stress-Transport (SST) turbulence model developed by Menter (1994), with again second-order accurate solutions for all variables.

3.2. *Numerical setup and boundary conditions*

As explained by Moreau *et al.* (2003) the flow around an airfoil when installed in a free-jet wind tunnel significantly deviates from that of the same airfoil placed in a uniform stream. The importance of accounting for these installation effects is more pronounced in the current study, as the wind tunnel jet dimension is relatively small compared to the

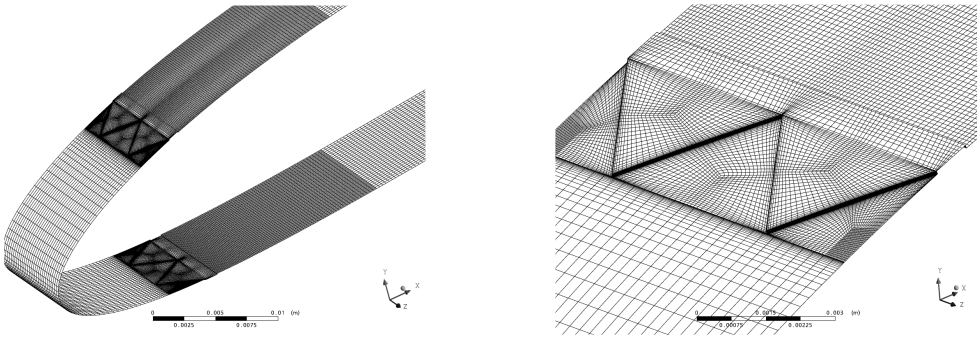

FIGURE 3. Left: Grid refinement on the airfoil for resolving the boundary-layer transition process. Right: Close-up view on the boundary-layer trip mesh region.

mock-up size and aspect ratio. The procedure is as described by Christophe & Moreau (2008). The LES domain size is 3.5 c in the streamwise (x) direction, c in the crosswise (y) direction and 0.074 c in the spanwise (z) direction. The latter is important for acoustic far-field computations, as will be discussed in Sec. 5. The LES boundary conditions are the steady RANS velocity profiles (U and V components) coming from the full wind tunnel simulation (Fig. 2, left) as inflow conditions along the whole extended C-contour (Fig. 2, right), a no-slip boundary condition on the airfoil surface, a convective outflow boundary condition at the wake exit and periodic conditions in the spanwise direction. The time step was chosen so that the convective Courant-Friedrichs-Lewy number (CFL) was about 1. At the interfaces of the refined grid, the CFL can locally reach values up to 10. The simulation ran for 11.67 flow-through times, based on the freestream velocity and airfoil chord length, before the solution reached a statistically steady state. Airfoil surface pressure and wake velocity statistics were then acquired for a period of eight flow-through times with a sampling rate of 50 kHz.

3.3. *Boundary-layer trips and grid topologies*

A block-structured C-mesh, shown in Fig. 2 (right), is used with $1112 \times 90 \times 32$ cells, similar to the initial LES on the CD airfoil by Wang *et al.* (2004). In the grid refinement region the spanwise extent is resolved with 80 grid points. A total of 300 streamwise grid points are placed in the wake region. The grid spacing on the airfoil ranges from $\Delta x/c = 5.2 \times 10^{-5}$ to 4.1×10^{-3}. The near-wall resolution is $y^+ \sim 0.5 - 1$. As suggested by Moreau *et al.* (2006), a smooth-grid distribution and orthogonality at the wall is applied and the grid-stretching is limited in both the streamwise and crossflow directions to ensure numerical stability.

To model the boundary-layer trip, two cases have been set up. First the actual serrated aluminum tape used in the experiments creates a 3-D disturbance in the flow. The region above and behind the trip has been resolved on a finer scale in the spanwise direction ($\Delta z/c = 9.3 \times 10^{-4}$) to better capture the expected transition process (Fig. 3, left). The finer resolved blocks have a streamwise extent of 190 trip thicknesses and a height of 19 trip thicknesses. The remaining grid has a spanwise resolution of ($\Delta z/c = 2.3 \times 10^{-3}$). A further run with a simplified step replacing the serrations, but of the same height and length (2-D disturbance), has been started. In that case no grid refinement was necessary.

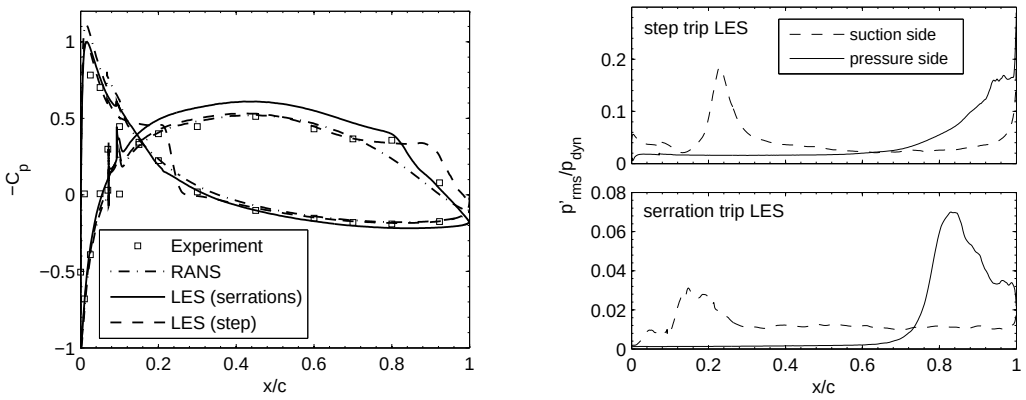

FIGURE 4. Left: Mean wall-pressure coefficient $-C_p$ on the airfoil. Right: root mean squared (rms) values of the pressure fluctuations along the chord for the step trip LES and the serration trip LES.

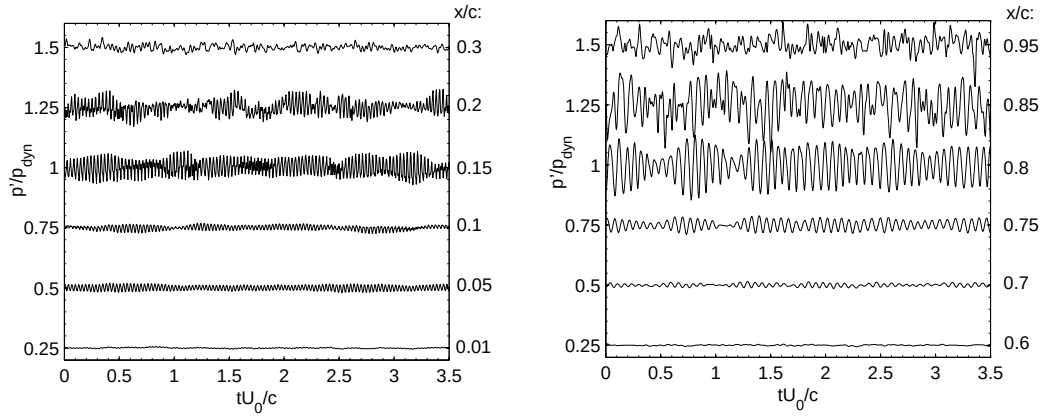

FIGURE 5. Airfoil wall-pressure fluctuations at different x/c locations. Left: Pressure side. Right: Suction side. Fluctuations are centered around artificial vertical offsets 0.25, 0.5, ..., 1.5.

4. Aerodynamic results

4.1. *Mean and fluctuating pressure distributions*

The calculated pressure distributions are compared to the experimental ones in Fig. 4. The RANS data (only the result from the whole wind tunnel setup is shown, the truncated 3-D domain gives almost identical values and is therefore omitted) are seen to agree fairly well with the measured pressure distribution. However, the separation occuring at approximately 0.8 c is missed. On the contrary, both LES capture this separation. Yet only the LES with the serrated trip predicts the separation location exactly but slightly deviates in the overall level of the pressure coefficient on the suction side for $x/c < 0.7$. The LES with the step trip delays this flow separation and also predicts an additional one on the pressure side observed neither in the experiment nor in the other LES. This could be attributed to the insufficient tripping effect of the step located just upstream of the separation bubble. The local experimental pressure peaks appearing in Fig. 4 (left) are caused by the boundary-layer trips on both airfoil sides.

In Fig. 4 (right), the pressure fluctuations on the airfoil reveal the effect of the boun-

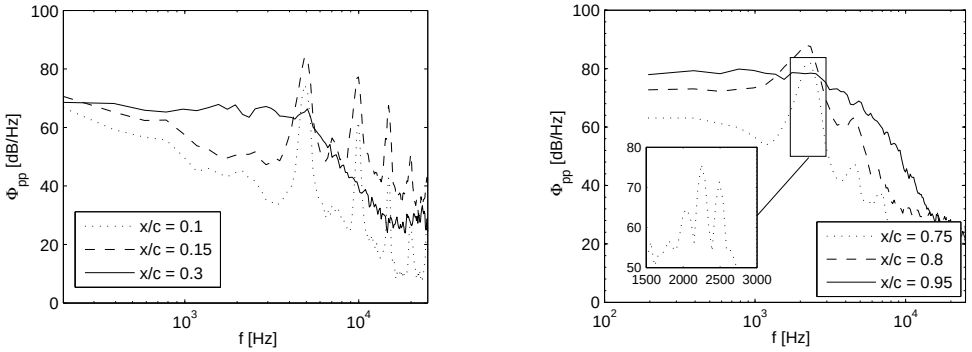

FIGURE 6. Wall-pressure spectra with reference to $2 \times 10^{-5} Pa$, at selected x/c locations. Left: Pressure side. Right: Suction side. The zoom window shows the broad spectral peak with higher resolution.

dary-layer trip. In the region of the boundary-layer trip (0.1 c), the root mean squared (rms) values of the pressure increase drastically on the pressure side, leading to a turbulent boundary layer for $x > 0.25$ c. On the suction side, however, the tripping does not induce direct transition. For the serrated trip LES the rms values increase sharply at x = 0.7 c, followed by separation and reattachment of the boundary layer. The peak occuring at 0.8 c agrees with the local loss of lift seen in Fig. 4 (left). For $x \geq 0.9$ c the boundary layer is turbulent and attached. For the step trip, the transition is triggered more smoothly and the peak is delayed to 0.9 c. In Fig. 5, the time history of the pressure fluctuations at different locations on both pressure (left) and suction (right) sides provides a further insight into the boundary layer transition process for the serrated trip case. Small quasi-periodic disturbances are strongly amplified during transition. Figure 6 provides the spectral content of these pressure signals. Narrow-band humps and their harmonics are seen whenever the observer point is in the transitional part of the boundary layer. Figure 6 also shows that on the pressure side, the broad peak occurs around 5000 Hz (left) and disappears for $x > 0.3$ c, whereas on the suction side the broad peak is centered around 2250 Hz (right). A higher resolution Fourier analysis not only reveals the broadband hump but also several tones on top of it. These tones coming from boundary-layer instabilities have been characterized experimentally by Arbey & Bataille (1983) among others, as well as recently with LES by Kim *et al.* (2006) and with DNS by Desquenes *et al.* (2007). The associated noise at discrete frequencies was also found to be partly caused by the separated flow close to the trailing edge. This discrete component signal indeed only exists approximately in the region $0.6\ c < x < 0.86\ c$ on the suction side. Figure 6 finally shows that at 0.95 c the attached boundary layer is fully turbulent and only broadband components are present in the spectrum on both, the pressure and suction sides. Yet the pressure fluctuations are much larger by approximately 10 dB on the suction side.

Figure 7 depicts relevant stations in the chordwise evolution of the wall-pressure space-time correlation on the airfoil pressure side (left) and suction side (right). Figure 7 (left) shows the space-time structures in the region close to the boundary-layer trip. The trip-induced instability turns the long structures observed at 0.01 c into a high-frequency oblique pattern at 0.05 c where the forward serrations of the trip are approximately located. Close to the trip end representing a backward-facing step, at 0.1 c, the observed

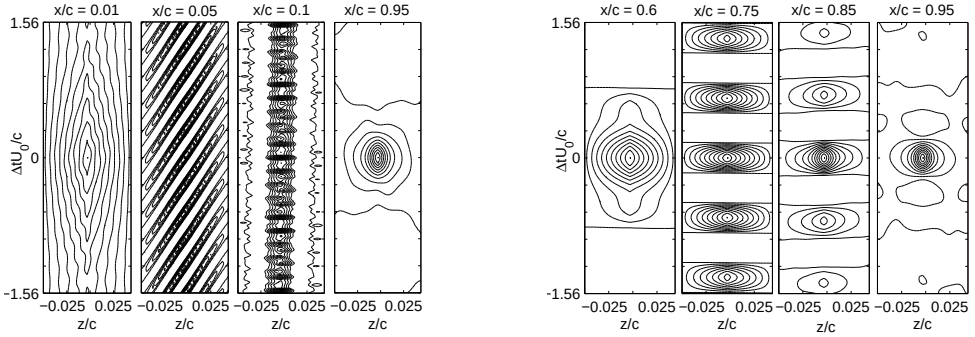

FIGURE 7. Space-time correlation of wall-pressure fluctuations at various x/c locations. Left: Pressure side. Right: Suction side. Contour values are from 0 to 0.9 with increment 0.1.

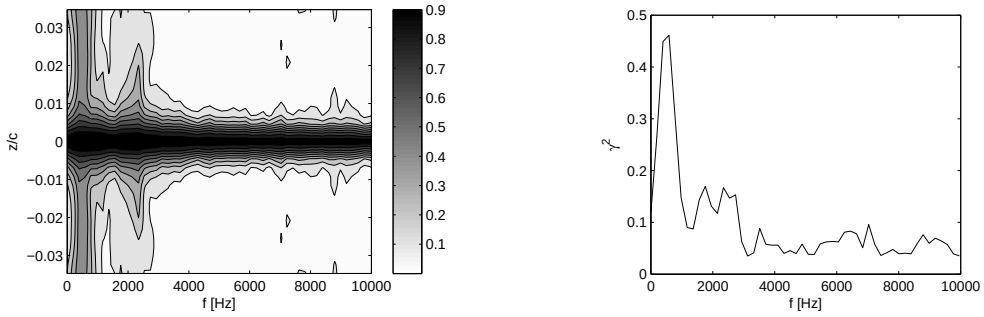

FIGURE 8. Pressure fluctuations at 0.95 c on the suction side. Left: Isocoherence values. Right: Variation of coherence with frequency for $\Delta z/c = 0.0278$.

pattern becomes spanwise rather compact and oriented in the streamwise direction. For $x > 0.3\ c$, it looks like that shown on the suction side near the trailing edge at 0.95 c. The boundary layer is fully turbulent and the respective structures are spanwise coherent. On the suction side the boundary layer begins destabilizing at 0.6 c and this instability is strongly amplified with a shorter time correlation at station 0.75 c (Fig. 7, right). This is evident from the periodic pattern observed in the timewise direction. The spanwise extent of these instabilities drops toward the trailing edge (0.85 c) and finally results in a spanwise compact finite domain in the attached boundary layer close to the trailing edge, similar to what was observed by Wang *et al.* (2004) on the CD airfoil at 8°.

Close to the trailing edge, the spanwise coherence function γ^2 also reveals if the computational domain size is large enough for the acoustic computations shown in the next section. Figure 8 (left) shows the spanwise distribution of γ^2 at different frequencies. At lower frequencies (< 800 Hz) the spanwise domain is not sufficiently large to allow for a decay of the coherence. The low-frequency components of the boundary layer are thus correlated over a much larger region than the higher frequency ones. Figure 8 (right) shows the coherence values for a spanwise separation of 0.0278 c. At approximately this location RMP measurements will be made to validate the current results.

4.2. *Velocity statistics in the wake*

All three velocity components have been extracted from the serrated trip LES and RANS results, in the airfoil wake at the same downstream locations as in the experiments. Fig-

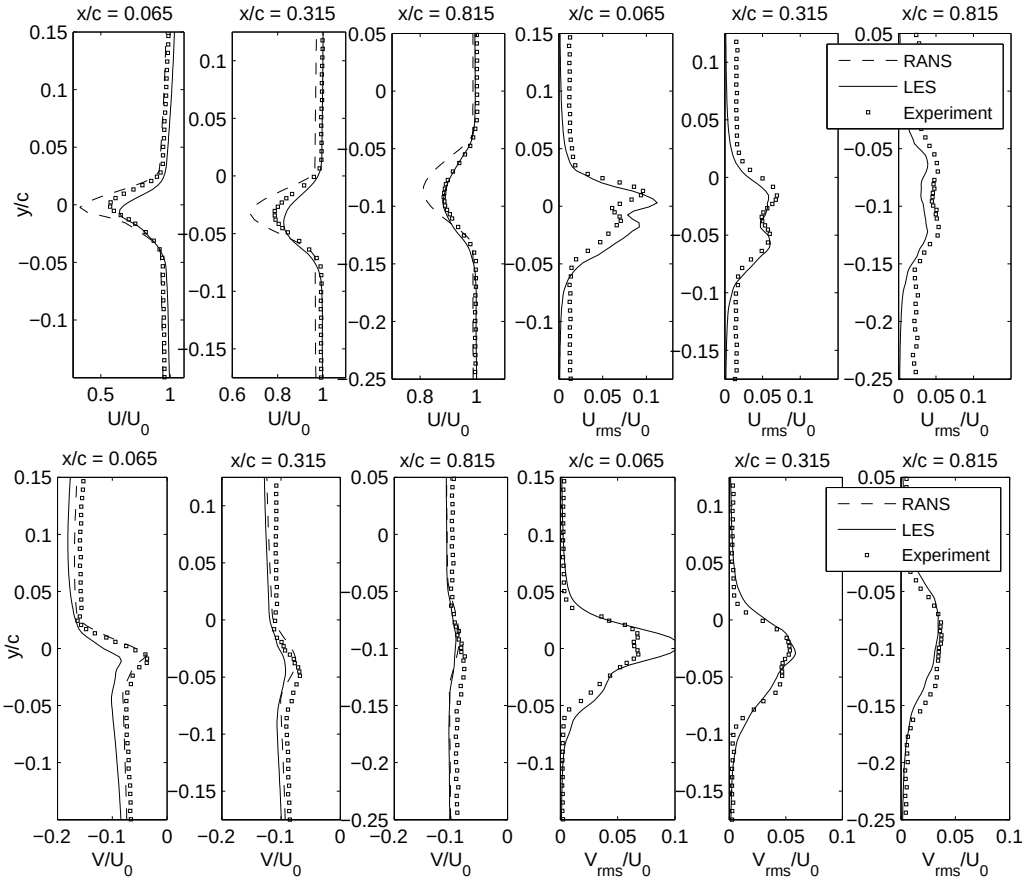

FIGURE 9. Normalized wake velocity data at three x/c locations. Top: Streamwise mean and rms velocity U/U_0 and U_{rms}/U_0. Bottom: Crosswise mean and rms velocity V/U_0 and V_{rms}/U_0.

ure 9 (left) shows the mean velocity profiles in streamwise (top) and crosswise (bottom) directions, together with the respective rms velocity profiles (right). For the streamwise component, a better agreement between LES and experiment is obtained further downstream: at 0.815 c downstream of the trailing edge, both curves almost collapse, showing the same wake width and depth. Further usptream the location of the maximum velocity deficit deviates by 12%, which might be attributed to insufficient spatial resolution of the hot-wire sensor in the region of strong velocity gradients, occuring in the very near-wake region. The RANS over-predicts the maximum deficit of the wake by 9–60% at all wake locations. The streamwise rms profiles, shown in Fig. 9 (top right) indicate that the LES captures the overall shape correctly, but not necessarily the magnitude. Yet the experimental background rms velocity values outside the wake are about 15% higher than in the LES, indicating perhaps the diffusion of turbulence from the nozzle shear layers into the jet core, or more likely a higher background turbulence level in the experiment. Similar observations can be made for the crosswise velocity components. Figure 10 (left) shows the wake deflection obtained by detecting the maximum wake deficit location at the eight streamwise measurement locations and fitting a linear curve by a

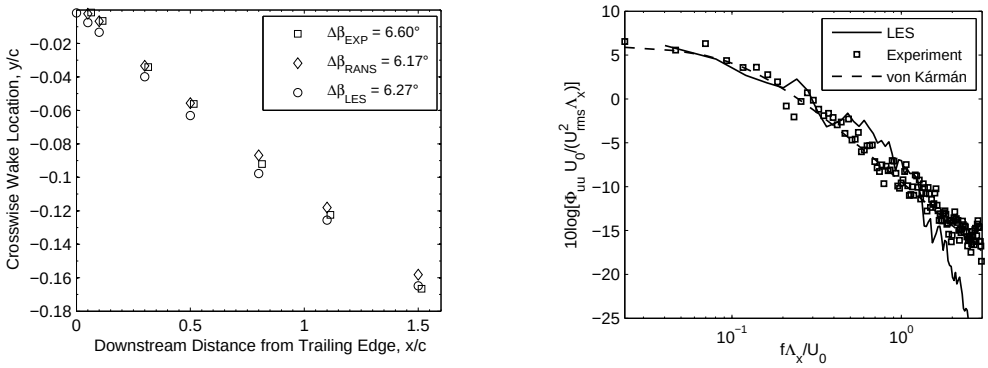

FIGURE 10. Mean and fluctuating velocities in the wake. Left: Mean flow deflection. Right: Streamwise velocity spectra.

least-squares method. Both RANS and LES results agree very well with the experiment, which substantiates the observations made in Fig. 4 (left) on the wall-pressure distribution. Thus, even though the RANS computations do not properly capture the wake width and depth, they do capture the wake deflection correctly. The non-dimensional streamwise turbulence energy spectrum in the maximum wake deficit at 0.015 c is shown in Fig. 10 (right). The spectra were obtained by dividing the data into eight records of equal length and applying a Hanning window with 50% overlap. They are normalized by the integral length-scale Λ_x. The experimental data have been re-sampled to the same resolution. The agreement between experiment and simulation is rather good, up to 8 kHz, above which the numerical grid cells act as a low-pass filter. Both spectra can be accurately modeled by a von Kármán spectrum.

5. Acoustic predictions

Trailing-edge noise computations are performed by two different methods based on Lighthill's (1952) acoustic analogy. First the formulation by Ffowcs Williams & Hall (1970) has been used, which assumes the airfoil to be a semi-infinite flat plate. Lighthill's equation is then solved using the exact Green's function. Details are given by Moreau *et al.* (2006). Second, the analogy by Curle (1955) is applied, which uses the free-space Green's function to give an integral solution to Lighthill's equation. In the presence of a rigid airfoil at a low Mach number, the farfield acoustic pressure, p_a, only involves a surface integral of the wall-pressure fluctuations. Furthermore, if the airfoil is assumed to be compact, retarded time variations can be neglected and p_a reads:

$$p_a\left(\vec{x},t\right) \approx \frac{r_i}{4\pi c_0 r^2} \oint_S \frac{\partial\left(n_j p'_{ij}\right)}{\partial t}\left(t-\frac{r}{c_0}\right) d^2\vec{y} \tag{5.1}$$

where r is the distance between source ($\vec{y}$) and observation point ($\vec{x}$). The contribution from the viscous stress tensor has been neglected. The time derivatives are approximated by a central differencing scheme. Pressure values for each radiating element are obtained at the element's center by linear interpolation from the values at the surrounding four nodes of each quadrilateral element. One limitation to Curle's approach is that it is strictly valid only for acoustically compact bodies, i.e., for acoustic wavelengths much larger than the airfoil chord ($\lambda >> c$), if the simulation is incompressible. If the body

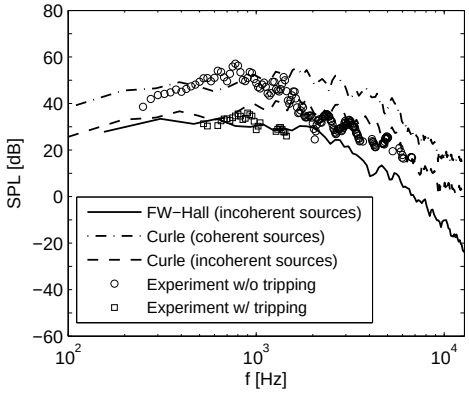

FIGURE 11. Sound-pressure levels in dB with $\Delta f = 3.125\ Hz$ and reference to $2 \times 10^{-5} Pa$. Predictions are from the serrated trip LES.

is non-compact, its surface extends into the acoustic farfield and the surface pressure can no longer be treated as incompressible. In that case, a tailored Green's function is required to obtain the correct solution. The source terms for Ffowcs Williams & Hall's method have been acquired at every time step for eight flow-through times in the LES case with serrations, leading to approximately 10320 values. The source terms for Curle's analogy are the surface pressure fluctuations, acquired every four time steps for the same LES and total length of eight flow-through times, leading to 2560 values. The total records are divided into eight segments for averaging. The discrete Fourier transform is performed in connection with a Hanning window. The experimental trailing-edge noise, as obtained from the correlation and filtering technique described earlier, is plotted in Fig. 11 in terms of its sound-pressure level (SPL). Two cases are presented, one with and one without boundary-layer tripping applied. There is a noticeable difference of approximately 10 dB between the two cases. Also, the frequency range of the assigned trailing-edge noise is slightly different in both cases. This is partly due to the low signal-to-noise ratio for the tripped case. For the acoustic prediction schemes, the far-field SPL for the whole airfoil span, L, have been calculated from the restricted span in the LES, L_{LES}, by assuming statistically independent acoustic source regions. This is valid whenever the simulation domain size is larger than the spanwise integral length-scale, i.e., when the coherence function drops to zero within the spanwise domain, see Wang & Moin (2000). From Fig. 8, it is evident that this is fulfilled for $f > 800\ Hz$. The total SPL of the airfoil for this incoherent source assumption is $(L/L_{LES}) \times SPL_{LES}$. Ffowcs Williams & Hall's method yields a rather good prediction of the acoustic far-field for the tripped boundary-layer case. Curle's method on the other hand over-predicts the SPL significantly and is in closer agreement to the untripped boundary-layer experimental data, for $f > 1\ kHz$. If one assumes a coherent source distribution along the span, which is valid whenever the spanwise integral length-scale is larger than the airfoil span, the SPL is $(L/L_{LES})^2 \times SPL_{LES}$ and Curle agrees with experimental data for $f < 1\ kHz$. Overall, Curle's method provides a reasonable prediction of the SPL, when switching between both solutions is considered. However, the tripping device does not seem to provide the required effect on the airfoil suction side: the far-field pressure prediction using Curle's analogy is in closer agreement to the untripped case than to the tripped one.

6. Conclusions and perspectives

A detailed flow analysis has been made, based on the LES of a NACA6512-63 at zero angle of attack. The original experimental boundary layer-trip serrations have been incorporated into the numerical grid. A simplified step trip has also been investigated. The wall-pressure data show that boundary-layer transition as well as flow separation occur on the airfoil. The wake-velocity profiles are predicted correctly by the serrated trip LES, in terms of wake width and depth. The agreement is found to improve with the downstream evolution of the wake. The RANS $k-\omega$ SST-model does not reproduce the correct wake width or depth, but agrees well with both, serrated trip LES and experiment, in terms of mean crosswise wake-velocity V, wake deflection and airfoil load. The LES with the exact serration trip not only agrees with the experimental lift but also predicts the correct separation point on the suction side. This feature was not captured by either the RANS simulation or the LES with the simplified step trip on the same grid. The wall-pressure spectra in the serrated trip LES furthermore suggest that close to the trailing edge, the boundary layer is turbulent and attached on both sides. In the transitional region, discrete frequency components have been observed that disappear after transition. Overall, the steady RANS inflow boundary conditions have proven to yield a correct lift distribution and wake deflection angle in the LES. Since the boundary layer is tripped artificially and the airfoil itself is within the potential core of the wind tunnel jet, neglecting the inflow turbulence is found to be a valid approximation for the present LES. The computational domain size was found to be too small to capture the spanwise coherence decay over all frequencies. For $f < 800\ Hz$, the coherence does not decay to zero. The implications of this to acoustic predictions have been found in the application of Curle's theory. If the source terms are assumed to be coherent, Curle's theory gives reasonable results for $f < 1\ kHz$, whereas for frequencies above $1\ kHz$ the incoherent source assumption is in closer agreement. This suggests that an interpolation between both results will yield an overall reasonable fit to the measured SPL. However, Curle's results agree only with the broadband noise of the untripped acoustic measurements, which are approximately 10 dB higher than the tripped results. Yet, Ffowcs Williams & Hall's theory provides a reasonable prediction of the tripped-airfoil sound radiation. The discrepancies between both methods need more investigation.

The LES with the simplified step, for which preliminary results have been presented, is still running to further explore how the boundary layer flow statistics are captured in this simplified case. A comparison with experimental wall-pressure spectra will be made to allow additional validation and assessment of the two current simulations.

Acknowledgments

The authors would like to thank Professor Parviz Moin for providing the necessary computational resources on the JHF cluster at Stanford University and the German Research foundation (DFG) for providing the financial support to the first author. Furthermore, the support of Professor Thomas Carolus at the University of Siegen and all the helpful discussions with him are gratefully acknowledged.

REFERENCES

Arbey, H. & Bataille J. 1983 Noise generated by airfoil profiles placed in a uniform laminar flow. *J. Fluid Mech.* **134**, 33–47.

Blake, W. K. & Lynch, D. A. 2002 Source characterization by correlation techniques. *Aeroacoustic Measurements*, Mueller, T. J., Editor. Berlin: Springer, 218–257, 2002. ISBN 3-540-41757-5.

Christophe, J. & Moreau, S. 2008 LES of the trailing-edge flow and noise of a controlled-diffusion airfoil at high angle of attack. *Proceedings of the Summer Program 2008*, Center for Turbulence Research, Stanford Univ./NASA Ames.

Curle, N. 1955 The influence of solid boundaries upon aerodynamic sound. *Proc. Roy. Soc. A* **231**(1187), 505–514.

Desquenes, G., Terracol, M. & Sagaut, P. 2007 Numerical investigation of the tone noise mechanism over laminar airfoils. *J. Fluid Mech.* **591**, 155–182.

Ffowcs Williams, J. E. & Hall, L. H. 1970 Aerodynamic sound generation by turbulent flow in the vicinity of a scattering half plane. *J. Fluid Mech.* **40**(4), 657–670.

Germano, M., Piomelli, U., Moin, P. & Cabot, W. H. 1991 A dynamic subgrid-scale eddy viscosity model. *Phys. Fluids A* **3**(7), 1760–1765.

Hama, F. R. 1957 An efficient tripping device. *J. Aero. Siences* **24**, 236–237.

Kim, H. J., Lee, S. & Fujisawa, N. 2006 Computation of unsteady flow and aerodynamic noise of NACA0018 airfoil using large-eddy simulation. *Int. J. Heat Fluid Flow* **27**(2), 229–242.

Lighthill, M. J. 1952 On sound generated aerodynamically I. General theory. *Proc. Roy. Soc. A* **211**(1107), 564–587.

Lilly, D. K. 1992 A proposed modification of the Germano subgrid-scale closure method. *Phys. Fluids A* **4**(3), 633–635.

Menter, F. R. 1994 Two-equation eddy-viscosity turbulence models for engineering applications. *AIAA J.* **32**(8), 1598–1605.

Moreau, S., Henner, M., Iaccarino, G., Wang, M. & Roger, M. 2003 Analysis of flow conditions in freejet experiments for studying airfoil self-noise. *AIAA J.* **41**(10), 1895–1905.

Moreau, S., Iaccarino, G., Kang, S., Khalighi, Y. & Wang, M. 2004 Numerical simulation of a low speed fan blade. *Proceedings of the Summer Program 2004*, Center for Turbulence Research, Stanford Univ./NASA Ames.

Moreau, S., Mendonca, F., Qazi, O., Prosser, R. & Laurence, D. 2005 Influence of turbulence modeling on airfoil unsteady simulations of broadband noise sources. *AIAA Paper 2005-2916*, Eleventh AIAA/CEAS Aeroacoustics Conference, Monterey, California, May 23–25.

Moreau, S., Neal, D., Khalighi, Y., Wang, M. & Iaccarino, G. 2006 Validation of unstructured-mesh LES of the trailing-edge flow and noise of a controlled-diffusion airfoil. *Proceedings of the Summer Program 2006*, Center for Turbulence Research, Stanford Univ./NASA Ames.

Wang, M. & Moin, P. 2000 Computation of trailing-edge flow and noise using large-eddy simulation. *AIAA J.* **38**(12), 2201–2209.

Wang, M., Moreau, S., Iaccarino, G. & Roger, M. 2004 LES prediction of pressure fluctuations on a low speed airfoil. *Annual Research Briefs 2004*, Center for Turbulence Research, Stanford Univ./NASA Ames.

Winkler, J. & Carolus, T. 2008 Concept, design and characterization of a small aeroacoustic wind tunnel facility with application to airfoil measurements. *Noise Control Eng. J. accepted for publication.*